Rosa Daschner, Holger Hewener, Wolfgang Bost, Steffen Weber, Steffen Tretbar and Marc Fournelle*

Ultrasound Thermometry for HIFU-Therapy

Abstract: High-Intensity Focused Ultrasound (HIFU) is an alternative tumour therapy with the ability for non-invasive thermal ablation of tissue. For a safe application, the heat deposition needs to be monitored over time, which is currently done with Magnetic Resonance Imaging. Ultrasound (US) based monitoring is a promising alternative, as it is less expensive and allows the use of a single device for both therapy and monitoring. In this work, a method for spatial and temporal US thermometry has been investigated based on simulation studies and in-vitro measurements. The chosen approach is based on the approximately linear dependence between temperature and speed of sound (SoS) in tissue for a given temperature range. By tracking the speckles of successive B-images, the possibility of detecting local changes in SoS and therefore in temperature is given. A speckle tracking algorithm was implemented for 2D and 3D US thermometry using a spatial compounding method to reduce artifacts. The algorithm was experimentally validated in an agar-based phantom and in porcine tissue for temperature rises up to △ 8°C. We used a focusing single element US transducer as therapeutic probe, a linear (/matrix array) transducer with 128 (/32·32) elements for imaging and thermocouples for validation and calibration. In all experiments, both computational and in-vitro, we succeeded in monitoring the thermal induced SoS changes over time. The in-vitro measurements were in good agreement with the simulation results and the thermocouple measurements (rms temperature difference = 0.53 °C, rms correlation coefficient = 0. 96).

Keywords: ultrasound thermometry, thermal strain, thermo-acoustic lens effect, plane wave compounding

https://doi.org/10.1515/cdbme-2021-2141

***Corresponding author: Marc Fournelle:** Fraunhofer Institute for Biomedical Engineering (IBMT), Joseph-von-Fraunhofer-Weg 1, 66280 Sulzbach/Saar, Germany
e-mail: marc.fournelle@ibmt.fraunhofer.de
Rosa Daschner, Holger Hewener, Wolfgang Bost, Steffen Weber, Steffen Tretbar: Fraunhofer Institute for Biomedical Engineering, Sulzbach/Saar, Germany

1 Introduction

Liver cancer has the third lowest survival rate among oncologic diseases [1]. The standard therapeutic procedures are associated with high risk of morbidity and mortality. Therefore, High-Intensity Focused Ultrasound (HIFU) has emerged as an alternative non-invasive therapy. [2] An associated problem concerns the need for monitoring and regulating the HIFU-induced heat deposition in a cost-effective and patient-friendly way. Ultrasound (US) thermometry meets the criteria as it allows the use of a single device for both therapy and monitoring. It furthermore is widely available and offers high spatial and temporal resolution. In this work, we studied a method for 2D and 3D US thermometry, that allows the determination of HIFU-induced temperature changes in biological tissue. The method is based on the thermal strain approach, that tracks the induced changes in the speed of sound (SoS) in tissue. In-vitro experiments were performed based on an agar-phantom and porcine tissue. For validation of the algorithm and the in-vitro results based on the agar-phantom, two computational model were used. One simulates the HIFU-induced temperature changes and one represents the US transducers used for US data acquisition. For the in-vitro measurements based on porcine tissue, calibration experiments were conducted, allowing the validation via thermocouples. In this work, the focus lies on the 2D implementation of the method. However, the suitability of the algorithm for 3D will be verified.

2 Methods

Thermal strain approach: Temperature changes in tissue cause variations in SoS and thermal expansion coefficient α_{th}. By assuming constant SoS c_0 for beamforming, temperature changes lead to image distortions called *thermal strains.* The eponymous thermal strain approach aims to detect local changes in SoS by tracking the associated speckle (= scatterer) shifts. The relation between the time shifts δt and the temperature changes ΔT is given by [3]:

$$\mathbf{\Delta T(z)} = \frac{\mathbf{1}}{\mathbf{2}} \frac{\mathbf{1}}{\boldsymbol{\alpha_{th}-\beta_{th}}} \frac{\boldsymbol{\partial(\delta t(z))}}{\boldsymbol{\partial z}}, \quad (1)$$

with axial depth z (m) and thermal strain $\frac{\partial(\delta t(z))}{\partial z}$ $(\frac{m}{s})$. The parameter $\beta_{th} = \frac{\partial(c(T))}{\partial T}$ represents the relationship between

SoS and temperature changes. For temperature rises up to 50 °C, β_{th} can be approximated linearly and prevails the value of α_{th} [4]. Temperatures above 25 °C are not considered in this work. Therefore, α_{th} is not considered. The speckle time shifts are determined by dividing the A-Scans of successive B-images in overlapping windows and correlating the corresponding ones. We used a kernel size of 8 λ (= wavelength) as proposed by Pernot et al.[5] and overlaps of 60 %.

Noise Reduction: The thermo-acoustic lens effect produces strong artifacts behind the heated areas of temperature images based on the thermal strain approach. Pernot et al. [5] attribute the cause to the fact that US cannot "see" behind these areas because it is distorted by the temperature changes. Therefore, they propose the use of spatial compounding techniques: By emitting plane waves under steering angles > 0°, US beams can reach behind the heated areas without passing them. The B-images obtained by beam steering can be compounded by coherent summation to form an image with information and quality gain. The estimated time shifts must be differentiated along the beam axis (see eq. 3). Therefore, compounding is applied on the thermal strains with the correlation strength of the time shifts considered as weighting factors:

$$\left[\frac{\partial(\delta t(x,y,z))}{\partial z}\right]_{\text{compound}} = \frac{\sum_{m=1}^{M} K_m(x,y,z)\frac{\partial(\delta t(x,y,z))}{\partial z}^{m}}{\sum_{m=1}^{M} K_m(x,y,z)\frac{\partial(\delta t(x,y,z))}{\partial z}}, \qquad (2)$$

where M represents the number of steering angles, K_m the corresponding correlation coefficient and x/y the lateral /elevational coordinate.

Numerical differentiation leads to additional noise [6]. Therefore, a combination of a threshold and median filter was implemented to filter the estimated time shifts.

HIFU and Imaging Model: The HIFU induced temperature distribution $T(x,y,z,t)$ can be described via Pennes' bio-heat equation [7], that considers the heat exchange between blood and tissue, heat conduction and heat generation by metabolism. In our case of ex-vivo tissue samples, the heat exchange can be neglected, and the heat generation is substituted by the heat deposition $Q\ (\frac{W}{m^3})$, which leads to:

$$\rho c \frac{\partial T}{\partial t} = \nabla(\lambda_T \nabla T) + Q \qquad (3)$$

where $\rho\ (\frac{kg}{m^3})$ is the density, $c\ (\frac{J}{kg \cdot K})$ the specific heat and $\lambda_T\ (\frac{W}{m \cdot K})$ the thermal conductivity of the tissue. The heat deposition is mainly affected by the HIFU-induced sound pressure p as follows:

$$Q = \alpha \frac{p^2}{\rho c}, \qquad (4)$$

with absorption coefficient α (Np).

The HIFU-induced pressure and temperature distributions were simulated using Matlab© toolbox k-wave. The pressure in the in-vitro measurements is not known, so a root-mean-square pressure of 1.8 MPa is assumed at the focus. To simulate the raw data acquisition, a defined number of point scatterers is randomly distributed in the modelled phantom. Each scatterer is randomly weighted, representing the strength of scattering. Using the relationship between time of flight and propagation distance for plane waves, the US echoes are calculated for every transducer element. $c(x,y,z) = c_0 + \beta_{th} * \Delta T(x,y,z)$ represents the HIFU-induced SoS distribution using the temperature distribution $\Delta T(x,y,z)$ of the thermal model, $\beta_{th} = 2\ \frac{m}{s \cdot °C}$ and $c_0 = 1540\ \frac{m}{s}$. Transducer transfer functions corresponding to them of the probes used in the experimental setup have been considered in the simulation.

3 Experimental Setup

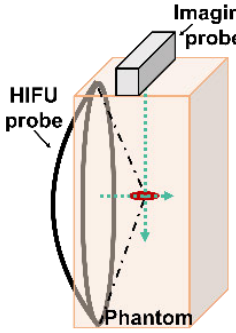

Figure 1: Experimental setup, US beam axis in green.

We used a focused single element US transducer (375 kHZ, Ø75 mm, 50 mm radius of curvature) as therapeutic probe, a linear/matrix array transducer (7/2.8 MHz, 128/32·32 elements, Vermon) and multichannel US research systems with single element channel data access (DiPhaS [8], Fraunhofer IBMT) for data acquisition. The imaging and HIFU transducers were placed orthogonally such that the acoustic axis of the imaging probe hits the focus of the HIFU probe (see Fig. 1). Due to the geometric conditions, the focus was located at a depth of about 50 mm of the image plane.

The agar-phantom was generated according to Kollman et al. [9] and has acoustic characteristics comparable to human tissue. In all cases, c_0=1540 $\frac{m}{s}$ was assumed. To ensure the coupling of the US to the test objects, the in-vitro measurements took place in a water bath. To avoid interferences, the HIFU-applications were interrupted for imaging. We used 9/25 steering-angles in the 2D/3D case in the range between -9.2° and +9.2°.

Validation via thermocouples: For validation, a thermocouple was inserted in the porcine tissue until it was visible in the B-image. To avoid miscalculations resulting from thermocouple artifacts and while assuming that the focus is symmetric with respect to the acoustic axis of the HIFU probe, positions on opposite sides of the HIFU transducer acoustic axis were compared for evaluation (thermocouple vs. US thermometry, see Fig. 5). The ROI detected by the thermocouple is assumed to be a circle with surface of 2 mm^2.

Calibration measurements: For calibration measurements (inspired by Anand et al. [10]) a slice of porcine tissue was placed in a water bath, that was gradually heated using a kettle. The tissue temperature was observed via thermocouples while raw data acquisition took place. The thermally induced shifts

Δz of a chosen event were estimated in A-Mode. The SoS changes Δc can be calculated by:

$$\Delta c = c(T + \Delta T) - c(T_0) = 2\frac{\Delta z}{t(T_0)}, \quad (5)$$

with initial temperature T_0. By linear regression β_{th} was determined to be 2.24 $\frac{m}{s\,°C}$ (see Fig. 2).

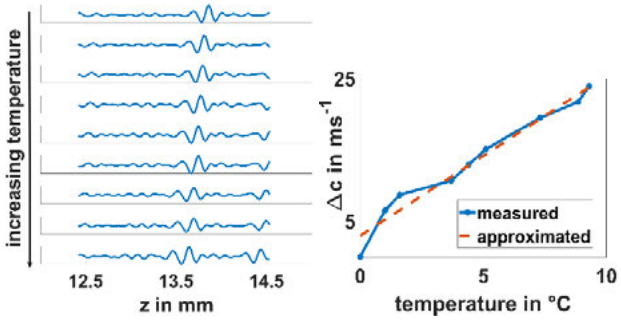

Figure 2: Experimental determination of β_{th}. Left: Measured A-lines. Right: linear approximation of β_{th}.

4 Results

The presented 2D images are aligned horizontally in lateral and vertically in axial direction. The unit is specified in millimeters. The color bars are scaled in temperature changes.

Agar-Phantom: To test the algorithm on the simulated US data, a HIFU-application time of 30 s was chosen. Fig. 3 shows the resulting temperature maps obtained by simulation (d), the reconstructed experimental data when using the thermometry algorithm without spatial compounding (a), with spatial compounding only (b) and with the additional filter (c). The artifacts decrease from a to c. For validation, a circular (/spherical) region of interest (ROI) was defined at the HIFU focus with a radius of 0.0025 m, in which the average temperature was calculated. The error is 0.13 °C/1.36 °C in the 2D/3D case.

Fig. 4 shows on the left the temperature map of the in-vitro measurement based on the agar-phantom after 30 s of HIFU-application. The heat accumulation at the focus is localized. Compared to Fig. 3c there is more noise. On the left,

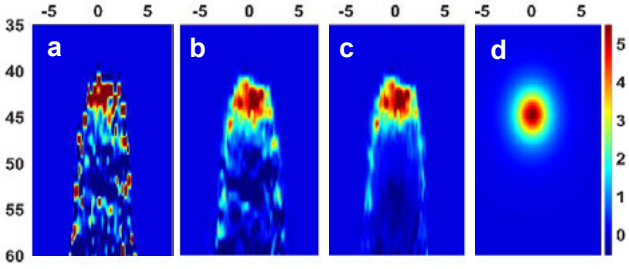

Figure 3: Development of the thermometry results (a-c) on simulated data based on the SoS distribution shown in d.

the normalized relative temperature changes over time are compared with these based on simulated US data. In both cases, the course rises sharply to a high value, followed by a rapid decrease.

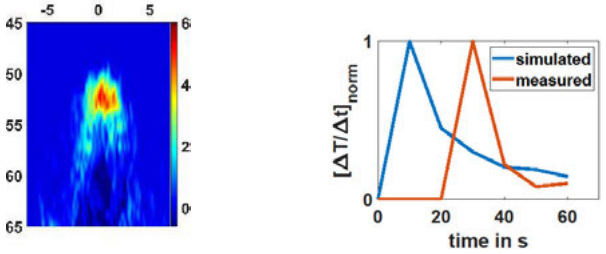

Figure 4: In-vitro measurements based on agar-phantom. Left: temperature map after 30 s of (real) HIFU application. Right: normalized relative temperature curves based on simulated (blue) and measured data (orange).

Porcine tissue: For the in-vitro measurements based on porcine tissue, HIFU-applications of 70 s were performed, which were interrupted every 10 s for US data acquisition. Three measuring series with inserted thermocouples were carried out. On average, a correlation of 96 % was obtained with a mean-root-square error of 0.53 °C and a standard deviation of 0.36 °C between the values of the US based thermometry and the thermocouple measurements. The individual results are listed in Table 1.

Fig. 5b shows the B-image of a measurement without inserted thermocouple with superposed thermometry results after 10 s of HIFU-application. A pronounced heat accumulation is seen at the focus. No characteristic artifacts of the thermo-acoustic lens effect are present.

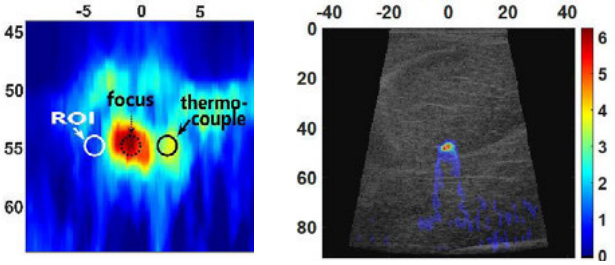

Figure 5: In-vitro measurements based on porcine tissue. Left: determination of ROI for thermocouple validation. Right: B-image with superposed temperature map.

Table 1: Validation of the US thermometry by comparing the measurements with those of the thermocouples.

Distance to HIFU focus	Correlation coefficient	Root-mean-square error	Standard deviation
0.004 m	0.99	0.22 °C	0.12 °C
0.003 m	0.92	0.41 °C	0.35 °C
0.002 m	0.93	0.95 °C	0.61 °C

3D: The 3D measurements with pork tissue were performed at half the frame rate of the 2D measurements. Fig. 6 shows the

3D temperature map in a reconstruction volume of 21 cm^3 (24· 24 · 36 mm^9) after a HIFU-application of 30 s with sectional view through the focus. The algorithm managed to locate the heat accumulation at the focus with temperatures approximately one third smaller than the ones of the 2D measurements.

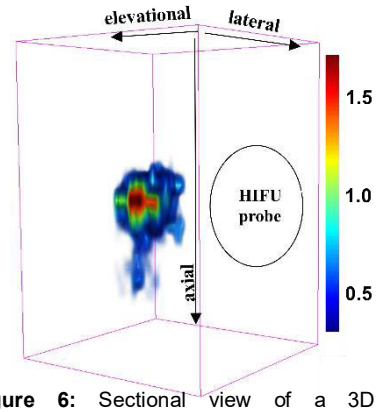

Figure 6: Sectional view of a 3D temperature map measured in pork tissue.

5 Discussion

In all measurements, the thermometry algorithm succeeded in localizing and tracking the HIFU-induced heat generation and the applied filter methods allowed reducing artefacts.

The US thermometry results based on the agar phantom were compared with the simulation results. The quantitative comparison is not possible due to the unknown value for β_{th}. Nevertheless, a qualitative comparison is possible. The estimated thermal course of the measured temperatures was shifted against the simulated one. One possible explanation is the interruptions of the HIFU-application, which gives time for cooling and are not considered in the simulation.

The US thermometry results based on porcine tissue were calibrated and validated in 2D using thermocouples. There is a high agreement and correlation between the measurement methods (> 90 %), which decreases with increasing proximity to the focus. The estimated temperatures in 3D were below those estimated in 2D. The deviations may partly result from the lower pixel / voxel size in the 3D reconstruction, which can affect the accuracy of summation during compounding.

Limitations: In this work, a limited temperature range is considered, in which a linear relationship between temperature and SoS changes can be assumed. For temperatures between 50 °C and 60 °C, an approximation with second order polynomials has proven to be effective [10]. Higher temperatures lead to necrosis and concomitant increasing decorrelation of the speckles, which distorts the temperature estimations [5]. The necrosis indicates the success of the therapy. Therefore, the detection of decorrelation may eliminate the need for temperature measurement in this range.

The test objects used in this work are inanimate phantoms. In the use case, breathing and perfusion movements of the patient can cause miscalculations in the estimated time shifts. To apply the thermometry algorithm to in vivo measurements, motion compensation must be considered, as well as a standard method for the determination of β_{th}.

6 Conclusion

In this work, a method for spatial and temporal US thermometry has been investigated and validated in 2D. Furthermore, the suitability of the implemented algorithm for 3D thermometry has been verified. However, the method must be extended to a temperature range up to the HIFU target temperature and motion compensation must be applied.

Author Statement
This work was supported by the Fraunhofer Internal Programs under Grant No. PREPARE 840232 THERANUS. Authors state no conflict of interest.

References

[1] Joint publication of the Center for Cancer Registry Data and the Society of Epidemiological Cancer Registries in Germany E.V.: Krebs in Deutschland (2015/16), 12th ed., RKI, 2020.
[2] Yufeng Zhou: Principles and Applications of Therapeutic Ultrasound in Healthcare. 1st ed. CRC Press, 2015.
[3] Simon C, VanBaren P, Ebbini ES: Two-dimensional temperature estimation using diagnostic ultrasound: IEEE Trans Ultrason Ferroelectr Freq Control 1998,45:1088-99.
[4] Lewis MA, Staruch RM, Chopra R: Thermometry and ablation monitoring with ultrasound, Int J Hyperthermia. 2015,31(2):163-181.
[5] Pernot M, Tanter M, Bercoff J Waters KR, Fink M: Temperature estimation using ultrasonic spatial compound imaging Trans Ultrason Ferroelectr Freq Control, 2004,51(5):606-15.
[6] Kallel F, Ophir J: A Least-Squares Strain Estimator for Elastography. Ultrasonic Imaging. 1997;19(3):195-208.
[7] Pennes HH: Analysis of tissue and arterial blood temperatures in the resting human forearm. Appl Physiol 1998,85(1):5-34.
[8] Risser C, Hewener H, Fournelle M, Fonfara H, Barry-Hummel S, Weber S, Speicher D, Tretbar S. Real-Time Volumetric Ultrasound Research Platform with 1024 Parallel Transmit and Receive Channels. Appl Sci. 2021;11(13):5795
[9] Kollmann C, Bezemer RA, Fredfeldt KE, Schaarschmidt UG, Teirlink CJPM: A Laminar Flow Test Object Based on the Draft IEC 61685 Standard for Quality Assurance of Ultrasound Doppler Equipment. Ultraschall Med. 1999;20(6):248-57.
[10] Anand A, Savery D, Hall C: Three-dimensional spatial and temporal temperature imaging in gel phantoms using backscattered ultrasound. IEEE Trans Ultrason Ferroelectr Freq Control. 2007,54(1):23-31